JOURNAL OF SOLID STATE CHEMISTRY **123,** 277–284 (1996)
ARTICLE NO. 0179

Supercritical Ammonia Synthesis and Characterization of Four New Alkali Metal Silver Antimony Sulfides: MAg_2SbS_4 and M_2AgSbS_4 (M = K, Rb)

George L. Schimek, William T. Pennington, Paul T. Wood, and Joseph W. Kolis[1]

Department of Chemistry, Clemson University, Clemson, South Carolina 29634-1905

Received September 5, 1995; accepted February 6, 1996

Four new semiconducting quaternary antimony sulfides, KAg_2SbS_4 (I), K_2AgSbS_4 (II), $RbAg_2SbS_4$ (III), and Rb_2AgSbS_4 (IV) were prepared in supercritical ammonia at 160°C in 4 days from the appropriate mole ratios of K_2S_4, K_2CO_3, or Rb_2CO_3 with Ag, Sb_2S_3, and S_8. Both silver-rich materials, I and III, crystallize in structure types previously observed in $BaAg_2GeS_4$ and $SrCu_2SnS_4$, respectively. However, it was determined that the space group of the latter compound was inaccurately reported in the literature. Novel structure types were obtained for II and IV. The structures of I–III contain three-dimensional anionic frameworks, either $[Ag_2SbS_4]^-$ or $[AgSbS_4]^{2-}$, built from a variety of edge- or vertex-shared antimony sulfide and silver sulfide tetrahedra. The alkali metal cations in I and II reside in two orthogonal, intersecting channels, and in three isolated one-dimensional channels in III. Compound IV has a layered structure, with a double layer of rubidium cations separating the neighboring anionic frameworks. It is noteworthy that I–III crystallize in noncentrosymmetric space groups. The structural diversity resulting from the condensation of quite regular SbS_4 and distorted AgS_4 tetrahedra in these four compounds and their optical band gaps are discussed. Crystal data: (I), red polyhedron, tetragonal space group, $I\bar{4}2m$, a = 6.886(1) Å, c = 8.438(2) Å, V = 400.16(9) Å^3, Z = 2, and $R(wR)$ = 0.0397(0.0335); (II), yellow plate, orthorhombic space group, $Pnn2$, a = 10.348(2) Å, b = 10.522(2) Å, c = 7.946(2) Å, V = 865.2(3) Å^3, Z = 4, and $R(wR)$ = 0.0377(0.0392); (III), yellow-orange needle, trigonal space group, $P3_221$, a = 6.630(1) Å, c = 16.700(2) Å, V = 635.8(2) Å^3, Z = 3, and $R(wR)$ = 0.0244(0.0310); (IV), yellow polyhedron, monoclinic space group, $P2_1/n$, a = 8.229(3) Å, b = 10.857(2) Å, c = 10.346(2) Å, β = 91.55(2)°, V = 924.0(4) Å^3, Z = 4, and $R(wR)$ = 0.0377(0.0405).

INTRODUCTION

Research efforts in this laboratory have centered upon the preparation of novel solid state compounds using supercritical (s.c.) solvents, in particular amines, as a reaction medium (1). A valuable property of s.c. solvents is that their very low viscosities allow them to act as transport media, and also enable them to solubilize normally intractable reagents (2). These properties are advantageous in that they often lead to high quality crystal growth. Furthermore, the variable s.c. temperatures of amines allow the desired reaction temperatures to be "dialed in," leading to a variety of kinetically stabilized materials.

We have found that one class of materials with a very rich chemistry in s.c. amines is quaternary alkali metal silver antimony sulfides. In this paper we report the synthesis of four new compounds in the M–Ag–Sb–S system from s.c. ammonia. They can be isolated in reasonable yield and are highly crystalline. The use of s.c. ammonia as a reaction medium leads to the synthesis of products which are substantially different from those found in other amine solvents. For example, the reaction of the same reagents in s.c. ethylenediamine results in the formation of a new alkali metal sulfosalt derivative with the formulation $M_2Ag_3Sb_3S_7$ (M = K or Cs) (3). Most of the compounds formed in s.c. ethylenediamine are considered to be sulfosalt derivatives. However, the materials produced in s.c. ammonia do not formally fall under the strictest definition of sulfosalts because they do not contain a trivalent pnictide with three coordinate pyramidal geometry, but rather tetrahedral SbS_4^{3-} building blocks are formed. The compounds reported can be generalized to two formulations, MAg_2SbS_4 and M_2AgSbS_4 (M = K or Rb), although they crystallize in four different structure types. Their synthesis, structure, and preliminary optical properties will be discussed in this paper.

EXPERIMENTAL

Synthesis

The potassium phases, KAg_2SbS_4 (**I**) and K_2AgSbS_4 (**II**), can be prepared as the major product from stoichiometric quantities of K_2S_4 (prepared by a modified literature technique, (4)) for **I** or K_2CO_3 (Mallinckrodt, 99.5%) for **II**, Ag

[1] To whom correspondence should be addressed.

0022-4596/96 $18.00

(Strem, 99.9%), Sb_2S_3 (Strem, 98%), and S_8 (Mallinckrodt, 99.9%). The reagents (molar ratios of 1:2:1:1 for **I** and 2:2:1:5 for **II**) were loaded into quartz tubes in an argon-filled drybox. The tubes were subsequently evacuated ($\sim 10^{-3}$ Torr), about 0.5 ml of NH_3 was distilled onto the reagents (~150 mg scale), and then they were frozen. After sealing and thawing the tubes, an approximately 40% fill of NH_3 was realized (tube volume *ca.* 1.3 ml). The quartz tubes were loaded into a Parr 4740 high pressure autoclave and counterpressured with 3300 psi of argon at room temperature. The autoclave was heated at 160°C for 4 days and then cooled to room temperature. Both reaction products contained significant contamination from the other member. The red polyhedra of **I** and yellow plates of **II** both grew on the tube walls and were also interspersed with brownish-red bulk product. Based on X-ray powder diffraction, using a Scintag XDS/2000 (Cu$K\alpha$ = 1.540562 Å), the microcrystalline bulk powder was found to be an intimate mixture of the potassium title phases. However, one strong peak at $2\theta \sim 5.8°$ remained unidentified and did not match any known phases containing any combination of the four constituent elements.

The rubidium phases, $RbAg_2SbS_4$ (**III**) and Rb_2AgSbS_4 (**IV**), were synthesized from stoichiometric quantities of Rb_2CO_3 (Strem, 99%), Ag, Sb_2S_3, and S_8. The reagents (molar ratios of 8:32:8:5 for **III** and 16:16:8:5 for **IV**) were loaded and synthesized in the same manner as **I** and **II**. Yellow-orange needles of **III** and yellow polyhedra of **IV** were found growing off the tube walls, away from the bulk product in both reactions. Based on X-ray powder diffraction, the tannish-red bulk powder was determined to be a mixture of the title phases and Ag_3SbS_3, pyrargyrite, a known mineral (5), as well as three strong reflections with $23° < 2\theta < 25°$. Again, no reported phases containing these elements could be matched to the extra diffraction peaks.

Optical band gaps for **I–IV** were determined from room temperature diffuse reflectance measurements over the 200–800 nm range on a Shimadzu UV3100 spectrophotometer equipped with an integrating sphere attachment. Barium sulfate was used as the reflectance standard. The inflection point of the first derivative curve (reflectance) versus energy was assigned as the band gap.

Structure Determination

Single crystals of **I–IV** were isolated by decanting the ammonia to one end of the reaction tube, freezing the solvent, and then scoring and opening the reaction vessel. The product was coated with Nujol before examination under a microscope, and under these conditions, the title phases appeared to be indefinitely stable. All crystals were mounted with epoxy in capillaries. The capillaries were then mounted on a Rigaku AFC7R four-circle diffractometer. At least 23 randomly located reflections from each compound were indexed to the reported lattice parameters. Data were collected to $2\theta = 50°$ using an ω-2θ scan mode at 16°/min ($\leq$3 rescans). Data were corrected for Lorentz and polarization effects. For **I** the extinction conditions, derived from the body-centering, and an inconclusive $N(Z)$ test allowed for seven possible space groups: $I4/mmm$, $I\bar{4}2m$, $I4mm$, $I422$, $I4/m$, $I\bar{4}$, or $I4$. The solution in $I\bar{4}2m$ gave the best refinement and is in agreement with the space group chosen for $BaAg_2GeS_4$ (6a). The reflection conditions for **II**, $h0l$: $h + l = 2n$ and $0kl$: $k + l = 2n$, and an $N(Z)$ test that indicated a noncentrosymmetric space group, explicitly defined one possible space group, $Pnn2$. The successful solution and refinement of the structure, and lack of mirror symmetry in the compound, verifies this space group choice. For **III**, an $N(Z)$ test that indicated a noncentrosymmetric space group, Laue symmetry of $\bar{3}m1$, and the reflection condition $000l$: $l = 3n$ implied one possible space group, $P3_221$ (or its enantiomer). For **IV**, the reflection conditions $h0l$: $h + l = 2n$ and $0k0$: $k = 2n$, uniquely conformed to $P2_1/n$. The structures were solved by direct methods, SHELXS-86 (7), and refined on $|F|$ with teXsan (8) or SHELXTL-PLUS (9) by least-squares, full-matrix techniques (10). Scattering factors for all atoms were taken from the source programs utilized (8, 9). A DIFABS (11) absorption correction was applied to isotropically refined data for **I** and **IV** and an empirical absorption correction (12) (psi scan) was applied to the data for **II** and **III**. A secondary extinction correction was applied to **II–IV**, due to poorly fit low order data, and resulted in improved F_o vs F_c and more well-behaved thermal motion on sulfur atoms. For the noncentrosymmetric compounds, the residuals of both structural configurations are reported. Table 1 contains these details of data collection and refinement for **I–IV**. Atomic coordinates and isotropic thermal parameters are given in Table 2. Bond distances and angles for **I–IV** are given in Tables 3 and 4, respectively. Structural information reported in Tables 2–4 is derived from the absolute configuration with a lower residual.

Supplementary tables include crystallographic and refinement details, anisotropic thermal parameters, complete bond distances and angles, and structure factors. Also included in the supplementary material are full thermal ellipsoid plots, the optical diffuse reflectance spectra, and the detailed space group analysis of $SrCu_2SnS_4$.[2]

[2] See NAPS document No. 05299 for 42 pages of supplementary materials. Order from ASIS/NAPS, Microfiche Publications, P.O. Box 3513, Grand Central Station, New York, NY 10163. Remit in advance $4.00 for microfiche copy or for photocopy, $7.75 up to 20 pages plus $.30 for each additional page. All orders must be prepaid. Institutions and Organizations may order by purchase order. However, there is a billing and handling charge for this service of $15. Foreign orders add $4.50 for postage and handling, for the first 20 pages, and $1.00 for additional 10 pages of material, $1.50 for postage of any microfiche orders.

TABLE 1
X-Ray Crystallographic Data[a]

Formula	KAg_2SbS_4	K_2AgSbS_4	$RbAg_2SbS_4$	Rb_2AgSbS_4
Formula weight	504.82	436.05	551.19	528.79
Crystal system	tetragonal	orthorhombic	trigonal	monoclinic
Space group (No.), Z	$I\bar{4}2m$ (#121), 2	$Pnn2$ (#34), 4	$P3_221$ (#154), 3	$P2_1/n$ (#14), 4
a (Å)	6.886(1)	10.348(2)	6.630(1)	8.229(3)
b (Å)	6.886(1)	10.522(2)	6.630(1)	10.857(2)
c (Å)	8.438(2)	7.946(2)	16.700(2)	10.346(2)
β (°)	90.	90.	90.	91.55(2)
Volume (Å^3)	400.16(9)	865.2(3)	635.8(2)	924.0(4)
Calculated density (g/cm^3)	4.189	3.347	4.319	3.801
Crystal dimensions (mm)	0.05 × 0.05 × 0.12	0.03 × 0.12 × 0.20	0.07 × 0.08 × 0.18	0.25 × 0.30 × 0.35
2θ range (°), octants	5–50, h, k, l: $h > k$	5–50, h, k, l	4–50, h, $\pm k$, $\pm l$	4–50, h, k, $\pm l$
Refl. collected (unique)	142 (127)	960 (924)	1698 (484)	1848 (1726)
Observed, $I > X\sigma(I)$, R_{int}	105, 2.0, na	698, 3.0, na	376, 3.0, 6.2%	1286, 3.0, 4.4%
Variables	13	75	39	74
μ, mm^{-1}	9.637	7.206	14.331	16.294
Transmission range	0.740–1.226	0.971–1.000	0.757–0.999	0.761–1.466
Secondary extinction ($\times 10^{-7}$)	na	3.26	6.50	6.35
R[b], R(enant)[c]	0.0378, 0.0397	0.0377, 0.0384	0.0244, 0.0279	0.0377, na
wR[d], wR(enant)[c]	0.0316, 0.0335	0.0392, 0.0396	0.0310, 0.0335	0.0405, na
S[e], S(enant)[c]	2.57, 2.73	2.93, 2.96	0.91, 1.06	2.92
Residual (e$^-$:Å^3), max shift	1.18/−1.23, 0.001	1.50/−0.96, 0.01	0.66/−0.64, 0.001	1.12/−1.26, 0.001

[a] All data was collected at 22°C with Mo$K\alpha$ radiation, λ = 0.7107 Å. Decay was $<\pm 2.2\%$.
[b] $R = \Sigma\,||F_o| - |F_c||/\Sigma\,|F_o|$.
[c] Residuals observed for the model compounds with the incorrect absolute structure.
[d] $wR = [\Sigma\, w\{|F_o| - |F_c|\}^2/\Sigma\, w|F_o|^2]^{1/2}$; $w = 1/\sigma^2\{|F_o|\}$.
[e] $S = [\Sigma\, (|F_o|_i - |F_c|_i)/\sigma_i]/(n - m)$; $i = 1$ to n.

RESULTS

Structure

*KAg_2SbS_4 (**I**).* Compound **I** is isostructural with both $BaAg_2GeS_4$ and $(NH_4)Ag_2AsS_4$ (6). KAg_2SbS_4 has an antimony–silver–sulfide framework with orthogonal, intersecting channels in which the potassium cations reside. These channels run parallel to the crystallographic a and b axes. The asymmetric unit contains one potassium and antimony atom, each residing on $\bar{4}2m$ sites, a silver atom on a $\bar{4}$ site, and a sulfur atom on a mirror plane. As viewed nearly parallel to the a axis in Fig. 1, the anionic framework is built from vertex-shared, alternating SbS_4 and AgS_4 tetrahedra, forming a flattened eight membered ring. The SbS_4 tetrahedra are quite regular, with all bond distances at 2.353(7) Å and bond angles of 108.7(1)° and 111.0(3)°. However, the AgS_4 tetrahedra, even with all the Ag–S bond distances at 2.603(2) Å, are very distorted with bond angles of 95.12(7)° and 145.2(3)°. These distorted AgS_4 units are observed in all four compounds reported here and have been observed previously in the two isostructural compounds, where bond angles vary from *ca.* 94° to 146° (6). The orthogonal rings, perpendicular to the a and b axes are connected via shared Sb and S atoms to generate a three-dimensional framework that is body-centered. All sulfur atoms are three coordinate, to an antimony and two silver atoms, with respect to the anionic framework. Alternatively, **I** can be described as sheets of vertex-shared AgS_4 tetrahedra fused as eight membered rings in the ab plane. These sheets are linked together via vertices along the c axis by antimony atoms which bridge across the silver sulfide rings. The cavities between the antimony atoms accommodate the potassium cations, which are eight coordinate to sulfur and are arranged in a compressed cubic geometry, with K–S bond distances of 3.219(7) Å (×4) and 3.478(6) Å (×4).

*K_2AgSbS_4 (**II**).* Compound **II**, K_2AgSbS_4, unlike KAg_2SbS_4, is built from both edge- and vertex-shared SbS_4 and AgS_4 tetrahedra to form a three-dimensional network with potassium cations occupying channels that run parallel to the a and b axes. Four of the ten unique atoms (K1, K2, Ag1, Ag2) reside on two different twofold rotation axes parallel to the c axis, while the remaining atoms are located in general positions. The anionic framework and channels, as viewed down the a or b axis are nearly identical, given their similar lattice dimensions and lattice symmetry as derived from *Pnn*2. Figure 2 shows the general channel morphology, as viewed down the b axis, in which a double row of cations reside. However, Fig. 2 does not do justice in revealing the connectivity of the anionic framework. That is, the ''anionic groups'' that appear to run parallel to the a or b axis are not simple chains, nor

TABLE 2
Atomic Coordinates and Equivalent Isotropic Thermal Parameters (Å²)

Atom	Wyckoff	*X*	*Y*	*Z*	U_{eq}[a]
			KAg_2SbS_4		
K1	2*a*	0	0	0	0.033(4)
Ag1	4*d*	0	0.5	0.25	0.053(1)
Sb1	2*b*	0	0	0.5	0.014(1)
S1	8*i*	0.3010(6)	−0.3010	0.1580(7)	0.023(2)
			K_2AgSbS_4		
K1	2*b*	0	0.5	0.758(1)	0.050(7)
K2	2*a*	0	0	0.448(1)	0.032(4)
K3	4*c*	0.2468(6)	0.2349(6)	0.948(2)	0.054(4)
Ag2	2*a*	0	0	0.9519(8)	0.061(2)
Ag1	2*b*	0	0.5	0.2249(6)	0.049(3)
Sb1	4*c*	0.7272(1)	0.7254(1)	0.4485	0.0182(7)
S1	4*c*	0.5500(5)	0.7051(5)	0.2672(7)	0.024(3)
S2	4*c*	0.7104(6)	0.5518(5)	0.6322(8)	0.024(3)
S3	4*c*	0.9238(5)	0.7208(6)	0.3037(8)	0.027(5)
S4	4*c*	0.7201(6)	0.9228(5)	0.5872(7)	0.025(3)
			$RbAg_2SbS_4$		
Rb1	3*b*	0.4430(3)	0.4430	0.5	0.030(1)
Ag1	6*c*	0.0979(2)	−0.2828(2)	0.5962(1)	0.044(1)
Sb1	3*a*	0.7218(2)	0	0.6667	0.014(1)
S1	6*c*	0.5066(5)	−0.0198(5)	0.5533(2)	0.022(1)
S2	6*c*	0.7598(5)	−0.3326(6)	0.6746(2)	0.021(1)
			Rb_2AgSbS_4		
Rb1	4*e*	0.8583(2)	0.9671(1)	0.4934(1)	0.0369(7)
Rb2	4*e*	0.3718(2)	0.9910(1)	0.2626(1)	0.0395(8)
Ag1	4*e*	0.8715(1)	0.9671(1)	0.2184(1)	0.0405(7)
Sb1	4*e*	0.14266(9)	0.77329(7)	0.96164(7)	0.0161(4)
S1	4*e*	0.0162(4)	0.7721(3)	0.1613(3)	0.025(1)
S2	4*e*	0.2578(4)	0.5770(3)	0.9419(3)	0.027(1)
S3	4*e*	0.9560(4)	0.8117(3)	0.7932(3)	0.024(1)
S4	4*e*	0.3375(4)	0.9286(3)	0.9496(3)	0.023(1)

[a] The equivalent isotropic temperature factor, U_{eq}, is defined as $\exp(-8\pi^2 U_{eq} \sin^2 \theta/\lambda^2)$ where $U_{eq} = 1/3\{\sum_i \sum_j (U_{ij} a_i^* a_j^* \mathbf{a}_i \cdot \mathbf{a}_j)\}$ and the summations of *i* and *j* range from 1 to 3.

colinear to an axis. Figures 3a and 3b show slices of the structure at $z \sim 0$ and $z \sim 1/2$. The evident building block in these views is formed from the condensation of three edge-shared MS_4 tetrahedra, $[AgSb_2S_8]^{5-}$, which run parallel to [110] or [1$\bar{1}$0], depending upon the layer. The $[AgSb_2S_8]^{5-}$ fragment is generated from the asymmetric unit by operation of a twofold axis parallel to the *c* axis, about the silver atom. This tri-tetrahedral building block is linked to other translationally generated $[AgSb_2S_8]^{5-}$ units through Ag2, via vertex-shared sulfur atoms, to create a layer. Applying the *n*-glide symmetry operator to this layer generates corresponding layers above and below the original layer, but oriented orthogonal to each other. The linking Ag2 atoms not only stitch the building blocks into layers, but also serve to connect the neighboring layers, above and below, via sulfides of the SbS_4 tetrahedra. The dissected layers show rectangular pockets in which three potassium cations (K2, K3, K3′) reside, however the cation channels run infinitely, parallel to the *a* and *b* axes. As shown in the polyhedral view of Fig. 3c, the shift in neighboring layers created by the *n*-glide operations generates an overall herringbone arrangement of the tri-tetrahedral units.

The SbS_4 tetrahedra are quite regular in **II**, with an average bond distance and bond angle of 2.344(6) Å and 109(3)°, respectively. Again, both the edge- and vertex-shared silver tetrahedra have very distorted bond angles, with Ag1 and Ag2 ranging from *ca.* 88° to 129° and 95° to 152°, respectively. Given these large distortions, the Ag–S bond distances are quite regular, averaging a long 2.662(7) Å for the edge-bridged Ag1 and 2.59(7) Å for the vertex linked Ag2. All sulfur atoms are two coordinate to metals of the anionic framework. The cations reside in the orthogonal, intersecting channels that run parallel to the *a* or *b*

TABLE 3
Selected Bond Distances (Å)

		KAg_2SbS_4	
Sb1–S1	2.353(7) ×4	K1–S1	3.219(7) ×4
Ag1–S1	2.603(2) ×4	K1–S1′	3.478(6) ×4
		K_2AgSbS_4	
Sb1–S1	2.342(6)	K2–S1	3.37(1) ×2
Sb1–S2	2.345(6)	K2–S2	3.37(1) ×2
Sb1–S3	2.338(6)	K2–S3	3.251(7) ×2
Sb1–S4	2.352(6)	K2–S4	3.205(7) ×2
Ag2–S1	2.661(6) ×2	K3–S1	3.404(9)
Ag2–S2	2.662(7) ×2	K3–S1′	3.36(1)
Ag1–S3	2.532(6) ×2	K3–S2	3.375(9)
Ag1–S4	2.654(6) ×2	K3–S2′	3.39(1)
K1–S1	3.146(6) ×2	K3–S3	3.599(9)
K1–S2	3.207(7) ×2	K3–S3′	3.37(1)
K1–S4	3.56(1) ×2	K3–S4	3.779(9)
		K3–S4′	3.33(1)
		$RbAg_2SbS_4$	
Sb1–S1	2.334(3) ×2	Ag1–S2′	2.739(4)
Sb1–S2	2.346(4) ×2	Rb1–S1	3.418(4) ×2
Ag1–S1	2.485(3)	Rb1–S1′	3.486(4) ×2
Ag1–S1′	2.776(3)	Rb1–S2	3.357(3) ×2
Ag1–S2	2.470(3)	Rb1–S2′	3.464(3) ×2
		Rb_2AgSbS_4	
Sb1–S1	2.338(3)	Rb1–S3	3.399(3)
Sb1–S2	2.343(3)	Rb1–S3′	3.564(3)
Sb1–S3	2.330(3)	Rb1–S4	3.361(3)
Sb1–S4	2.332(3)	Rb1–S4′	3.764(3)
Ag1–S1	2.507(3)	Rb2–S1	3.278(3)
Ag1–S2	2.563(3)	Rb2–S1′	3.892(4)
Ag1–S3	2.794(3)	Rb2–S2	3.396(3)
Ag1–S4	2.664(3)	Rb2–S2′	3.709(4)
Rb1–S1	3.467(4)	Rb2–S3	3.371(3)
Rb1–S1′	3.692(4)	Rb2–S3′	3.480(4)
Rb1–S2	3.446(3)	Rb2–S4	3.313(3)
Rb1–S2′	3.604(4)	Rb2–S4′	3.405(3)

TABLE 4
Selected Bond Angles (°)

	KAg_2SbS_4		
S1–Sb1–S1	108.7(1) ×4	S1–Ag1–S1′	145.2(3) ×2
S1–Sb1–S1′	111.0(3) ×2	Sb1–S1–Ag1	109.0(1) ×2
S1–Ag1–S1	95.12(7) ×4	Ag1–S1–Ag1	138.5(3) ×2
	K_2AgSbS_4		
S1–Sb1–S2	104.7(2)	S3–Ag1–S4′	95.1(2) ×2
S1–Sb1–S3	112.1(2)	S1–Ag2–S1′	113.0(3)
S1–Sb1–S4	110.1(2)	S2–Ag2–S2′	114.9(4)
S2–Sb1–S3	110.8(2)	S1–Ag2–S2	128.4(2) ×2
S2–Sb1–S4	113.2(2)	S1–Ag2–S2′	88.4(2) ×2
S3–Sb1–S4	106.0(2)	Sb1–S1–Ag2	83.5(2)
S3–Ag1–S3′	151.4(3)	Sb1–S2–Ag2	83.4(2)
S4–Ag1–S4′	131.3(3)	Sb1–S3–Ag1	114.3(2)
S3–Ag1–S4	96.6(2) ×2	Sb1–S4–Ag1	119.4(2)
	$RbAg_2SbS_4$		
S1–Sb1–S1′	108.7(2)	S1′–Ag1–S2	90.3(1)
S2–Sb1–S2′	109.4(2)	S1′–Ag1–S2′	147.6(1)
S1–Sb1–S2	109.3(1) ×2	Sb1–S1–Ag1	103.1(1)
S1–Sb1–S2′	110.0(1) ×2	Sb1–S1–Ag1′	120.4(1)
S1–Ag1–S1′	91.6(1)	Ag1–S1–Ag1′	132.6(1)
S2–Ag1–S2′	94.9(1)	Sb1–S2–Ag1	111.3(1)
S1–Ag1–S2	105.4(1)	Sb1–S2–Ag1′	114.6(1)
S1–Ag1–S2′	113.7(1)	Ag1–S2–Ag1′	132.4(1)
	Rb_2AgSbS_4		
S1–Sb1–S2	105.7(1)	S1–Ag1–S4	120.5(1)
S1–Sb1–S3	111.9(1)	S2–Ag1–S3	113.4(1)
S1–Sb1–S4	112.0(1)	S2–Ag1–S4	118.1(1)
S2–Sb1–S3	110.9(1)	S3–Ag1–S4	104.0(1)
S2–Sb1–S4	111.2(1)	Sb1–S1–Ag1	84.8(1)
S3–Sb1–S4	105.2(1)	Sb1–S2–Ag1	82.0(1)
S1–Ag1–S2	85.79(9)	Sb1–S3–Ag1	114.0(1)
S1–Ag1–S3	115.0(1)	Sb1–S4–Ag1	115.4(1)

axis, the latter shown in Fig. 2. The K1 cation is located between adjacent SbS_4 tetrahedra, as viewed down the *b* axis. It is six coordinate to sulfur, arranged in a distorted bicapped tetrahedron, with an average bond distance of 3.3(2) Å. Cation K2 is located in a bicapped trigonal prismatic environment of sulfur atoms with an average bond distance of 3.30(8) Å. K3 is found in a distorted pentagonal bipyramid of sulfur atoms with an average K–S bond distance of 3.40(9) Å and one longer contact at 3.779(9) Å.

$RbAg_2SbS_4$ (***III***). Compound **III**, $RbAg_2SbS_4$ ($P3_221$), has many structural similarities with $SrCu_2SnS_4$ (14) ($P3_1$), and a detailed study revealed that $SrCu_2SnS_4$ is isostructural to **III** (*vide infra*). The asymmetric unit contains five unique atoms, three on general positions and Rb1 and Sb1 residing on two different twofold rotation axes. The anionic network in **III** is formed from the condensation of SbS_4 and AgS_4 tetrahedra, creating infinite channels in which the rubidium cations reside. An eight membered ring, consisting of alternating vertex-shared antimony- and silver-sulfide tetrahedra, forms the channel. This ring is generated

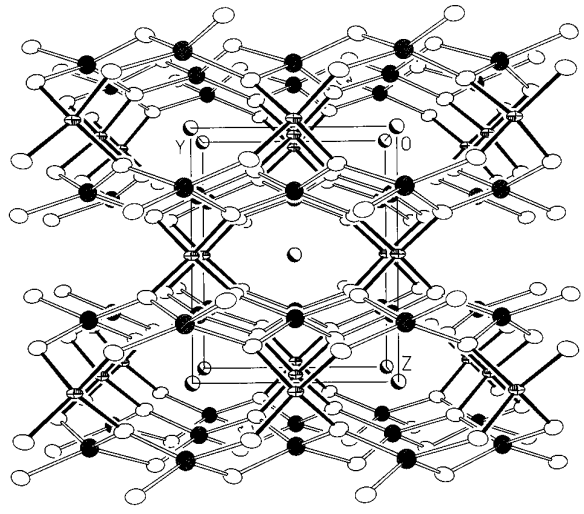

FIG. 1. View of the unit cell found in KAg_2SbS_4 (**I**), nearly parallel to the *a* axis. Antimony atoms are 70% probability thermal ellipsoids, silver atoms are solid spheres, potassium cations are highlighted spheres, and sulfur atoms are 70% probability boundary ellipsoids. Antimony–sulfur bonds are filled and silver–sulfur bonds are open.

from the asymmetric unit by applying twofold rotation symmetry operators. The sulfur atoms of the Sb and Ag tetrahedra are vertex-shared in such a way that the anionic framework becomes a network of fused columns. As shown in Fig. 4, the channels parallel to the *a* axis are clearly evident. Consecutive application of the 3_2 screw axis parallel to the *c* axis will bring into focus the channels parallel to the *a*–*b* bisector and then the *b* axis. Thus, each unit cell contains three nonintersecting channels at different *z* values which are shifted by 120° in the *ab* plane with respect to the channels above and below it. The SbS_4 tetrahedra

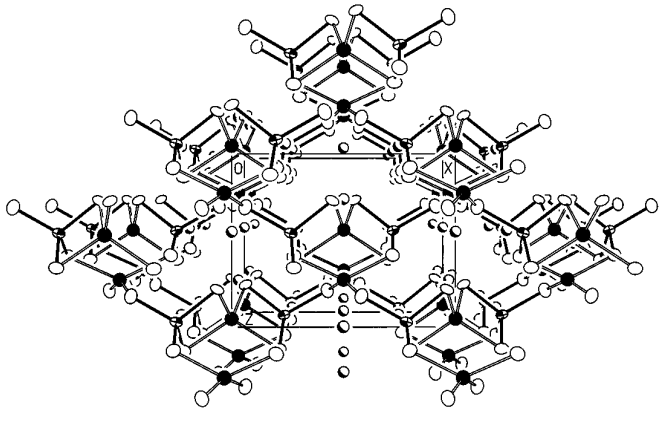

FIG. 2. View of the unit cell found in K_2AgSbS_4 (**II**) down the *b* axis. Cationic channels with similar morphology run parallel to the *a* axis and orthogonally intersect with those shown here. Atom types are the same as Fig. 1.

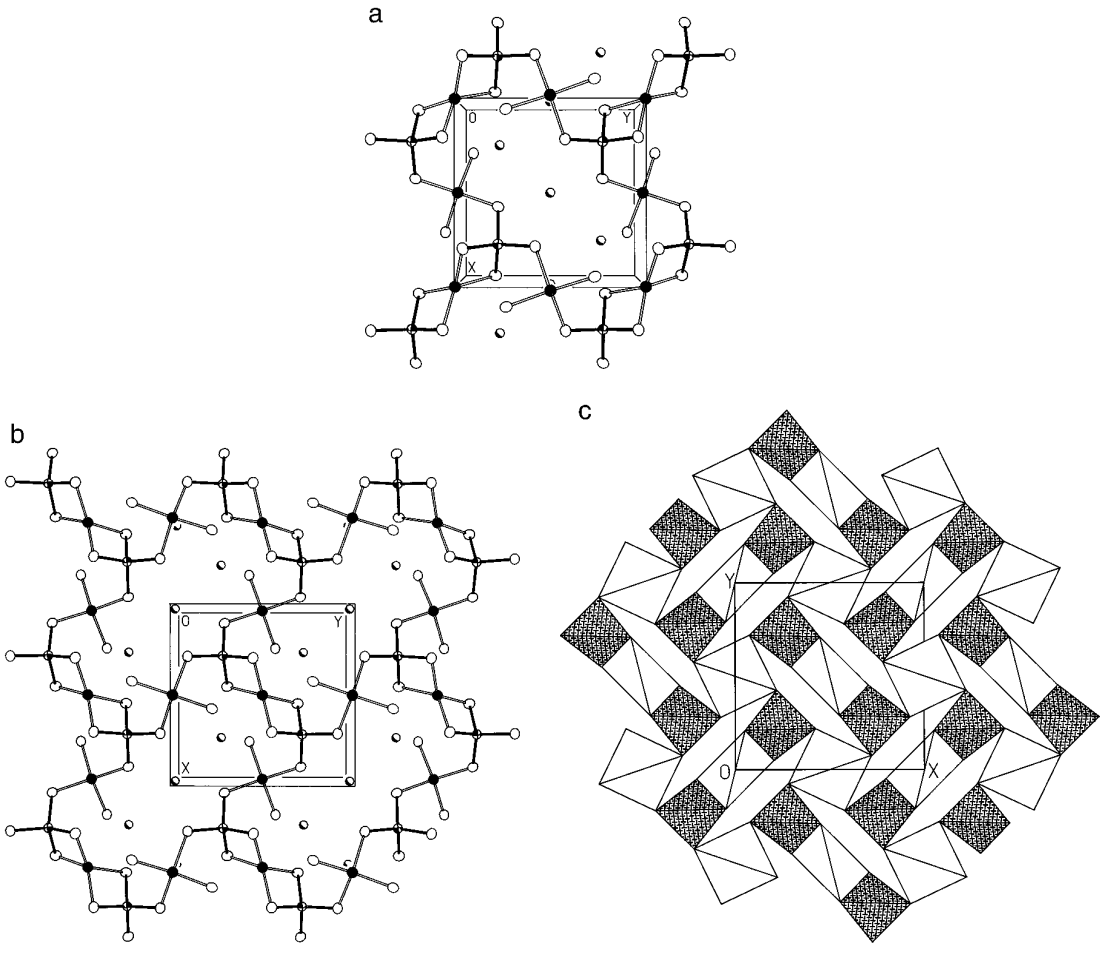

FIG. 3. A slice of the anionic framework at (a) $z \sim 0$ and (b) $z \sim 1/2$ in K_2AgSbS_4 (**II**). Note the $[AgSb_2S_8]^{5-}$ tri-tetrahedra linked via vertex-shared Ag(I) cations, which further serve to connect neighboring layers above and below. Potassium cations are located approximately above and below all silver and antimony atoms. Atom types are the same as Fig. 1. (c) A polyhedral view, down the *c* axis highlighting the herringbone arrangement of tri-tetrahedra, antimony tetrahedra are hatched and silver tetrahedra are open.

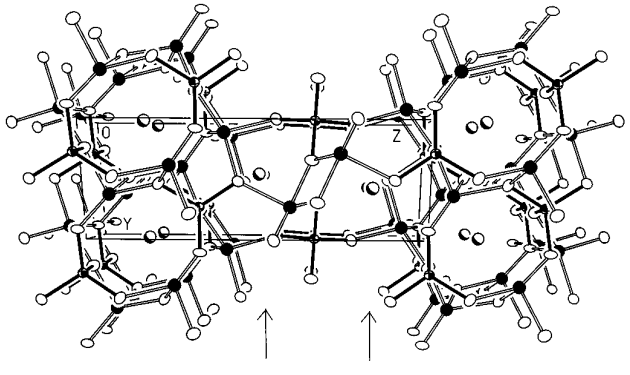

FIG. 4. Unit cell view of $RbAg_2SbS_4$ (**III**) down the *a* axis. Tunnels running parallel to the *b* axis and the *a*–*b* bisector are indicated by the arrows and are parallel to the viewing direction when the 3_2 screw axis symmetry operator is applied. Atom types are the same as Fig. 1.

again are quite regular ($\overline{d}$(Sb–S) = 2.339(6) Å and ∡(S–Sb–S) = 109.5(5)°) while the AgS_4 tetrahedra are very distorted ($\overline{d}$(Ag–S) = 2.6(2) Å and ∡(S–Ag–S) range from 90.3(1)° to 147.7(1)°). Both unique sulfur atoms are three coordinate to the anionic framework, to one antimony and two silver atoms. The one unique Rb is located in the tunnel. It has eight contacts to sulfur that range from 3.357(3) to 3.486(4) Å, arranged in a flattened square antiprismatic coordination geometry.

Rb_2AgSbS_4 (***IV***). Rb_2AgSbS_4 is the only centrosymmetric member in this series and contains a layered anionic framework separated by a double layer of Rb cations. All atoms reside on general positions. The Sb and Ag sulfide tetrahedra are linked together in a different fashion than **I–III**; however, they possess the common motif of edge- and vertex-shared tetrahedra. Each anionic layer is a condensation of SbS_4 tetrahedra via silver atoms, as shown in Fig. 5a. The SbS_4 tetrahedra are coordinated through the

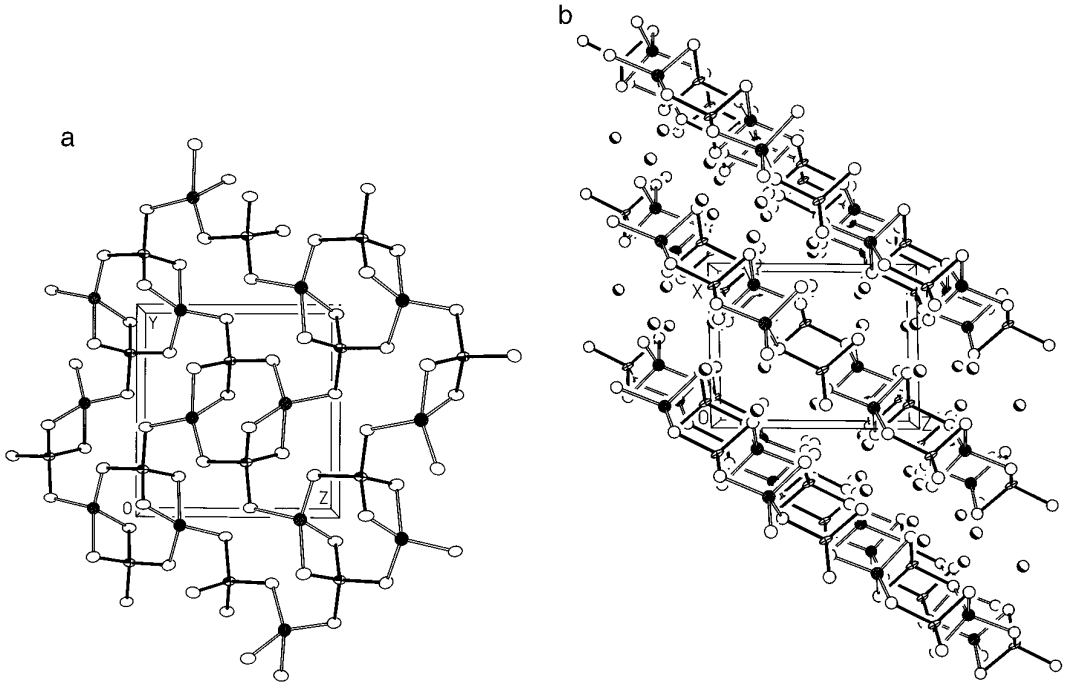

FIG. 5. (a) The anionic layer found in Rb_2AgSbS_4 (**IV**), showing the edge- and vertex-bridging tetrahedra of antimony and silver sulfide. Atoms types are the same as Fig. 1. (b) Arrangement of the layers in the unit cell of **IV** as viewed down the *b* axis.

sulfur atoms by three silver atoms, one edge-bridging and two vertex-sharing. This arrangement allows silver atoms to also be in a tetrahedral environment, although again, quite distorted. The edge-bridged silver–sulfur bonds (Ag1–S3 and Ag1–S4) are quite long and the vertex-shared sulfur atoms (S1 and S2) have contacts to silver atoms that are more typical. Once again the SbS_4 tetrahedra are quite regular, with an average bond distance and bond angle of 2.336(6) Å and 109(3)°, respectively, while the AgS_4 tetrahedra are distorted ($\overline{d}$(Ag–S) = 2.6(1) Å and ∡(S–Ag–S) = 109(13)°). All unique sulfur atoms are two coordinate to a silver and antimony atom in the anionic framework. The layers traverse the [101] plane, and are separated by a double layer of rubidium cations, as shown in the unit cell view of Fig. 5b. The shortest interlayer sulfur–sulfur contacts are about 3.24 Å. Both unique rubidium cations are eight coordinate to sulfur and arranged in a very distorted cubic geometry with $\overline{d}$(Rb1–S) = 3.5(1) Å and $\overline{d}$(Rb2–S) = 3.5(2) Å.

DISCUSSION

The utilization of supercritical NH_3 has afforded the synthesis of four new alkali metal silver antimony sulfides. Unlike $BaAg_2GeS_4$ and $SrCu_2SnS_4$ (or $SrCu_2GeS_4$, $BaCu_2GeS_4$, $BaCu_2SnS_4$ (15)) which were prepared above 550°C, their analogs, **I** and **III**, can be made at much lower temperatures (*ca.* 160°C). This low temperature regime may provide the kinetic stabilization necessary for the formation of such closely related products: **II** with **I** and **IV** with **III**.

All the anionic frameworks reported here are built from nearly ideal SbS_4 and distorted AgS_4 tetrahedra with varying degrees of condensation, either through edge- or vertex-bridging. Two different three-dimensional Ag–Sb–S anionic frameworks have been formed with the incorporation of the relatively small potassium cation. The isostructural arsenic analog of **I** has also been prepared, structurally characterized, and its optical band gap measured (16). In this work, the larger rubidium cation is found in one three-dimensional (**III**) and one two-dimensional (**IV**) framework of Ag–Sb–S. The role of cation size has been discussed in the literature (17), and a general inverse correlation between cation size and dimensionality has been observed. We have found, however, that we can prepare Rb, K and Rb, Cs analogs of **IV** and they are essentially isostructural with Rb_2AgSbS_4 (18). However, if both cation sites are substituted with Cs(I) to form Cs_2AgSbS_4, novel one-dimensional anionic chains are formed (19). This is not unexpected, given the increase in ionic radius of 0.19 Å when going from Rb(I) to Cs(I) (20). It should be noted, however, that a reduction in dimensionality is not observed in supercritical ethylenediamine chemistry, where the anionic frameworks of $Cs_2Ag_3Sb_3S_7$ and $CsAgSb_4S_7$ are complex two-dimensional layers (3).

Optical diffuse reflectance measurements on **I–IV** indicated that all four phases are semiconducting materials.

TABLE 5
Bond Valence Sums for MAg_2SbS_4 and M_2AgSbS_4 Phases

	I	II	III	IV
M	1.17(2)	1.04(2) 1.29(3) 0.90(2)	1.02(1)	1.03(1) 1.27(1)
Ag	1.08(6)	1.13(2) 0.92(2)	1.12(1)	1.04(1)
Sb	4.77(9)	4.88(8)	5.02(4)	5.00(4)

Band gaps of 2.2, 3.8, 2.3, and 3.9 eV for **I–IV**, respectively, were derived from the inflection point of the first derivative curve (reflectance) versus energy. In addition, all four compounds are electron precise, with the expected oxidation states: *M*(I), Ag(I), Sb(V), and S^{2-}, and are in agreement with their semiconducting optical band gaps. Bond valence sums, calculated from an empirical relationship between bond length and bond strength, as developed by Brown and Altermatt (21), are listed in Table 5 and are in agreement with expectations.

During a routine literature search, similarities in the lattice parameters and coordination geometries between $RbAg_2SbS_4$ (**III**) and $SrCu_2SnS_4$ (14) were noted. However, the latter compound was refined in $P3_1$, as reported in the literature, while the space group $P3_221$ was chosen for **III**. Through a judicious choice of the asymmetric unit in $SrCu_2SnS_4$, the missing twofold symmetry could be observed visually. From this asymmetric unit, an origin shift and appropriate orientation of the twofold axis resulted in atomic positions valid for the space group $P3_121$ in which Cu1/Cu2, S1/S2, and S3/S4 are related. Conversion of these atomic coordinates, necessary for the enantiomeric space group $P3_221$, resulted in positional parameters similar to **III**, as reported in Table 6. Thus, we believe that the appropriate space group choice for $SrCu_2SnS_4$ (and the later reported isostructural members $SrCu_2GeS_4$, $BaCu_2GeS_4$, $BaCu_2SnS_4$ (15)) is actually $P3_221$ or its enantiomer $P3_121$. A more detailed description of the transformation is included in the supplementary material.

TABLE 6
Relationship of Atomic Coordinates for $RbAg_2SbS_4$ and $SrCu_2SnS_4$

Atom	*X*	*Y*	*Z*	Atom	*X*	*Y*	*Z*
Rb1	0.4430	0.4430	0.5000	Sr1	0.4398	0.4398	0.5000
Sb1	0.7218	0.0000	0.6667	Sn1	0.7069	0.0000	0.6686
Ag1	0.0979	−0.2828	0.5962	Cu2	0.0750	−0.3432	0.5900
Ag1′	0.3807	0.2828	0.7371	Cu1	0.4197	0.3442	0.7459
S1	0.5066	−0.0198	0.5533	S1	0.4542	−0.0369	0.5497
S1′	0.5264	0.0198	0.7800	S2	0.4931	0.0379	0.7891
S2	0.7598	−0.3326	0.6746	S4	0.7616	−0.3505	0.6683
S2′	0.0925	0.3326	0.6588	S3	0.1123	0.3506	0.6707

ACKNOWLEDGMENTS

We are indebted to the National Science Foundation and the Petroleum Research Fund, administered by the ACS, for support of this research.

REFERENCES

1. (a) J. E. Jerome, P. T. Wood, W. T. Pennington, and J. W. Kolis, *Inorg. Chem.* **33,** 1733 (1994); (b) P. T. Wood, W. T. Pennington, and J. W. Kolis, *J. Am. Chem. Soc.* **114,** 9233 (1992).
2. A. Rabenau, *Angew. Chem. Int. Ed. Engl.* **24,** 1026 (1985).
3. G. L. Schimek, J. E. Jerome, W. T. Pennington, and J. W. Kolis, submitted for publication.
4. F. Feher, *in* "Handbuch der Preparativen Anorganischen Chemie" (G. Brauer, Ed.), pp. 280–281. Fedinand Enke, Stuttgart, Germany, 1954.
5. D. Harker, *J. Chem. Phys.* **4,** 381 (1936).
6. (a) Chr. L. Teske, *Z. Naturforsch. B* **34,** 544 (1979); (b) M. Auernhammer, H. Effenberger, E. Irran, F. Pertlik, and J. Rosenstingl, *J. Solid State Chem.* **106,** 421 (1993).
7. G. M. Sheldrick, *in* "Crystallographic Computing 3" (G. M. Sheldrick, C. Krüger, and R. Goddard, Eds.), pp. 175–189. Oxford University Press, London, 1985.
8. "teXsan: Single Crystal Structure Analysis Software, Version 1.6b." Molecular Structure Corporation, The Woodlands, TX 77381, 1993.
9. G. M. Sheldrick, "SHELXTL-PLUS." Siemens Analytical X-ray Instruments, Inc., Madison, WI 53719.
10. W. R. Busing, K. O. Martin, and H. A. Levy, "ORFLS, A FORTRAN Crystallographic Least Squares Program." Report ORNL-TM-305, Oak Ridge National Laboratory, Oak Ridge, Tennessee, 1962.
11. N. Walker and D. Stuart, *Acta Crystallogr. Sect. A* **39,** 158 (1983).
12. A. C. T. North, D. C. Phillips, and F. S. Mathews, *Acta Crystallogr. Sect. A* **24,** 351 (1968).
13. C. K. Johnson, "ORTEP-II, A FORTRAN Thermal Ellipsoid Plot Program." Report ORNL-5138, Oak Ridge National Laboratory, Oak Ridge, Tennessee, 1976.
14. Von Chr. L. Teske, *Z. Anorg. Allg. Chem.* **419,** 67 (1976).
15. (a) Chr. L. Teske, *Z. Naturforsch. B* **34,** 386 (1979); (b) Von Chr. L. Teske and O. Vetter, *Z. Anorg. Allg. Chem.* **426,** 281 (1976).
16. KAg_2AsS_4: $I\bar{4}2m$, a = 6.7504(5) Å, c = 8.265(1) Å, Vol = 376.61(8) Å^3, $R(\omega R)$ = 0.0520(0.0524), E_g = 2.25 eV. G. L. Schimek and J. W. Kolis, unpublished results.
17. M. G. Kanatzidis, *Phosphorus, Sulfur, Silicon, Relat. Elements* **93–94,** 159 (1994).
18. $RbCsAgSbS_4$: $P2_1/n$, a = 8.449(2) Å, b = 10.934(1) Å, c = 10.427(2) Å, β = 91.77(2)°, Vol = 962.8(3) Å^3, $R(wR)$ = 0.0222(0.0178), and $RbKAgSbS_4$: $P2_1/n$, a = 8.188(2) Å, b = 10.751(2) Å, c = 10.265(2) Å, β = 91.68(2)°, Vol = 903.3(3) Å^3, $R(wR)$ = 0.0372(0.0335). G. L. Schimek and J. W. Kolis, unpublished results.
19. P. T. Wood, G. L. Schimek, and J. W. Kolis, *Chem. Mater.* in press.
20. R. D. Shannon, *Acta Crystallogr. Sect. A* **32,** 751 (1976).
21. I. D. Brown and D. Altermatt, *Acta Crystallogr. Sect. B* **41,** 244 (1985).